Spin correlations and reentrant spin-glass behavior in amorphous Fe-Mn alloys. II. Dynamics

G. Aeppli
Brookhaven National Laboratory, Upton, New York 11973
and AT&T Bell Laboratories, Murray Hill, New Jersey 07974

S. M. Shapiro
Brookhaven National Laboratory, Upton New York 11973

R. J. Birgeneau
Department of Physics, Massachusetts Institute of Technology, Cambridge, Massachusetts 02139

H. S. Chen
AT&T Bell Laboratories, Murray Hill, New Jersey 07974
(Received 29 July 1983)

Inelastic-neutron-scattering measurements have been performed on amorphous $(Fe_{1-x}Mn_x)_{75}P_{16}B_6Al_3$ alloys for several concentrations x bracketing the spin-glass—ferromagnetic multicritical point found from magnetization measurements. For $x=0.35$, the alloy is nonferromagnetic, and the inelastic spectra are dominated at all temperatures by a resolution-limited quasielastic peak. We find no evidence for propagating modes of any kind. In a 10-kG applied field, the central peak is substantially reduced, and dispersionless sidebands, centered at the Larmor precession frequency, appear. Three samples ($x=0.30$, 0.25, and 0.20) on the ferromagnetic side of the phase diagram have also been studied. Spectra were collected for one of these ($x=0.25$) above its Curie point. These data are consistent with ordinary spin diffusion. For all three samples, resolvable spin-wave peaks exist at temperatures below the Curie points but above the spin-glass transitions established in bulk measurements. As the temperature is reduced, the spin-wave stiffness first increases, as in normal ferromagnets, and then decreases. At the lowest temperatures, resolvable spin-wave peaks are absent, and the spectra are dominated by a resolution-limited (<30 μeV full width at half maximum) quasielastic peak. For the most iron-rich material ($x=0.20$), true inelastic scattering coexists with the central peak, even at 5 K. This inelastic scattering broadens and decreases in intensity with increasing momentum transfer Q, in a manner consistent with simple spin-wave theory. The central-peak intensity decays according to a power law $Q^{-\alpha}$, with $\alpha \gtrsim 2$. At temperatures near the spin-glass—to—ferromagnetic crossover, direct inspection of the raw data for $x=0.20$ unambiguously demonstrates the coexistence of the central peak with well-resolved spin-wave peaks. Our experimental results are discussed in terms of existing theories on the dynamics of spin-glasses and ferromagnets with frozen-in disorder. Also included are speculations on time-dependent random fields, and their relevance to the crossover from ferromagnetic to spin-glass—like behavior.

I. INTRODUCTION

In an earlier paper[1] (hereafter referred to as paper I) we presented a small-angle neutron scattering (SANS) study of the spin correlations in amorphous $(Fe_{1-x}Mn_x)_{75}P_{16}B_6Al_3$ alloys. According to magnetization measurements,[2,3] these alloys exhibit spin-glass (SG), ferromagnetic (FM), and paramagnetic (PM) phases as a function of temperature T and manganese concentration x. Of particular interest is the crossover from FM to SG behavior, occurring as T is reduced in samples with $0.15 \lesssim x \lesssim 0.35$. We also observed this crossover in our SANS spectra, which at low temperatures assume a shape significantly different from that associated with normal ferromagnets.

The subject of the present paper is an inelastic neutron scattering study of the spin dynamics of amorphous $(Fe_{1-x}Mn_x)_{75}P_{16}B_6Al_3$. Similar studies have already been performed for several magnetic alloys displaying spin-glass—like behavior at low temperatures and ferromagnetism at higher T. The first and most dramatic results have been reported for polycrystalline Fe_xCr_{1-x},[4] which displays an FM to SG crossover with decreasing T for $0.2 \lesssim x \lesssim 0.3$. The inelastic neutron scattering measurements show that for $x \geq 0.26$, well-defined spin waves exist for T between the Curie temperature T_C and the spin-glass "transition" temperature T_g found from bulk measurements. As T was decreased from T_C, their energies initially increased, as they should in a normal ferromagnet. However, as T approached T_g, the spin-wave energies and lifetimes decreased to such an extent that at the lowest temperatures, no resolvable spin-wave peaks

remained. Analogous results have since been obtained for the metallic alloys Fe_xAu_{1-x} (Ref. 5) and $(Fe_xNi_{1-x})_{75}P_{16}B_6Al_3$.[6] A neutron scattering study of the spin dynamics of insulating $Eu_xSr_{1-x}S$ near its PM-FM-SG multicritical point has also been carried out.[7] The inelastic spectra here were dominated by an intense resolution-limited peak centered at zero-energy transfer. Although some true inelastic scattering was also observed, no resolvable spin-wave peaks were found *at any temperature* for the sample ($x=0.52$) which was thought at the time to display reentrant SG behavior. However, this result is consistent with a more recent high-resolution neutron-diffraction study, which has demonstrated the absence of true long-range FM order in a single crystal of $Eu_{0.52}Sr_{0.48}S$.[8]

In paper I we have already pointed out why the FM to SG crossover in $(Fe_{1-x}Mn_x)_{75}P_{16}B_6Al_3$ is very suitable for neutron scattering investigation. Specifically, the FM-SG-PM multicritical point occurs for an Fe concentration $1-x=0.65$, which is *three* times higher than in any other Fe-based alloy studied by this technique to date; this means that in the region of interesting magnetic behavior, the magnetic scattering intensity can be substantially larger. Also because of the higher spin density, the characteristic temperatures and excitation energies are higher. Obviously, both of these features make inelastic neutron scattering experiments easier to perform.

For the reader's convenience, we show again in Fig. 1 the magnetic phase diagram of $(Fe_{1-x}Mn_x)_{75}P_{16}B_6Al_3$. The solid lines represent the transition temperatures established from a scaling analysis of ac susceptibility and dc magnetization measurements.[2] As a function of temperature, the SANS intensity measured at constant momentum transfer $\vec{Q}$ exhibited two anomalies.[1] The first of these, at higher T, corresponds to the Curie point and is indicated by the solid circles in Fig. 1. The second, indicated by the open circles, occurs near the FM-SG crossover temperature given by the bulk measurements. We emphasize that SANS data are collected for finite momentum transfers ($|\vec{Q}|>0.01$ Å^{-1}), and consequently do not bear a model-independent relation to the results obtained using macroscopic techniques.

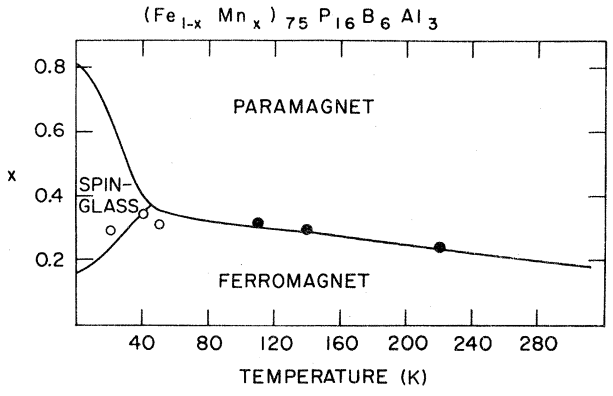

FIG. 1. Magnetic phase diagram for $(Fe_{1-x}Mn_x)_{75}P_{16}B_6Al_3$. Solid lines are from Ref. 2. Closed circles represent Curie temperatures T_C obtained from our SANS data (Ref. 1), open circles, the positions of the low-temperature anomalies in the $Q=0.02$ Å^{-1} SANS data.

We have performed inelastic neutron scattering measurements for one sample ($x=0.35$) on the spin-glass side of the phase diagram and three samples ($x=0.30$, 0.25, and 0.20) on the ferromagnetic side. For all samples, we have studied the temperature dependence of the scattering in the spin-glass and ferromagnetic regimes indicated in Fig. 1. The scattering in the paramagnetic regime was briefly surveyed for $x=0.35$ and 0.25. Finally, we have carried out a preliminary investigation of the effects of an applied magnetic field for $x=0.35$.

This paper is organized as follows. In the next section, we give a detailed description of the inelastic neutron scattering cross section for random ferromagnets and spin-glasses. Section III deals with our experimental technique and the procedures followed in the data analysis. In Sec. IV, we present the data and the results of the analysis. Section V contains a discussion which is divided into two parts. The first (subsection A) reviews existing theories on the dynamics of spin-glasses and random ferromagnets, and relates our experimental results to these theories. The second (subsection B) gives an account of how the random-field effects discussed in paper I might influence the spin dynamics of reentrant spin-glass (RSG) alloys. Finally, Sec. VI is a summary of our experimental results and suggests directions for future research.

II. NEUTRON SCATTERING CROSS SECTION

The neutron scattering technique measures directly the Fourier transform in space and time of the spin-spin correlation function.[9] The cross section can be written as

$$\frac{\partial^2\sigma}{\partial\Omega\,\partial E}=\left[\frac{\gamma e^2}{m_e c^2}\right]^2\frac{|\vec{k}_f|}{|\vec{k}_i|}\,|\tfrac{1}{2}gf(\vec{Q})|^2\times\sum_{\alpha,\beta}(\delta_{\alpha\beta}-\hat{Q}_\alpha\hat{Q}_\beta)S^{\alpha\beta}(\vec{Q},\omega)\,, \tag{1}$$

where

$$S^{\alpha\beta}(\vec{Q},\omega)=\frac{1}{2\pi}\int dt\,\exp(-i\omega t)\times\sum_{m,n}\exp[i\vec{Q}\cdot(\vec{r}_m-\vec{r}_n)]\times\langle S_m^\alpha(t)S_n^\beta(0)\rangle\,. \tag{2}$$

In Eq. (1), $\vec{k}_i$ and $\vec{k}_f$ denote the wave vectors of the ingoing and outgoing neutrons, respectively; $\vec{Q}=\vec{k}_f-\vec{k}_i$, $\hat{Q}=\vec{Q}/|\vec{Q}|$, and $f(\vec{Q})$ refers to the atomic form factor of the magnetic species; in Eq. (2), $\vec{r}_m$ represents the positions of the spin $\vec{S}_m$. The correlation function is a sum of contributions due to dynamic (oscillatory and relaxational) processes and the equilibrium arrangement of the spins:

$$S^{\alpha\beta}(\vec{Q},\omega)=\frac{\chi_0^{-1}\hbar\omega/kT}{1-\exp(-\hbar\omega/kT)}\delta^{\alpha\beta}[(1-\delta^{\alpha z})\chi_\perp(\vec{Q})F_\perp(\vec{Q},\omega)+\delta^{\alpha z}\chi_{||}(\vec{Q})F_{||}(\vec{Q},\omega)]+\delta(\omega)\tilde{S}^{\alpha\beta}(\vec{Q})\ . \tag{3}$$

χ_0 is the susceptibility of the free ions, and is usually proportional to $(kT)^{-1}$. We are considering disordered Heisenberg ferromagnets, so $\chi_\perp(\vec{Q})$ and $\chi_{||}(\vec{Q})$ are the zero-frequency susceptibilities measured perpendicular and parallel to the magnetization vector. $F_\perp(\vec{Q},\omega)$ and $F_{||}(\vec{Q},\omega)$ are the corresponding spectral functions, whose integrals with respect to ω are unity. Finally, $\tilde{S}^{\alpha\beta}(\vec{Q})$ is the *static* (infinite time) spin-spin correlation function. In this section, we discuss in more detail first the dynamic and then the static terms in Eq. (3).

We begin with the transverse susceptibility $\chi_\perp(Q)$, which is due to spin waves and generally takes the form (for small $\vec{Q}$)

$$\chi_\perp(\vec{Q})=\chi_0\frac{A_s}{Q^2}\ , \tag{4}$$

where, ordinarily, $A_s\sim T$. For $\vec{Q}=\vec{0}$, spin waves correspond to uniform rotation of all of the spins in the system. Because of the rotational symmetry of the Heisenberg Hamiltonian, such a rotation, even when it has an arbitrarily small amplitude, costs no energy. Consequently, as is evident from Eq. (4), $\chi_\perp(\vec{Q})$ diverges as $\vec{Q}\to\vec{0}$ for all $T<T_C$. Note incidentally that it makes no sense to define $\chi_\perp$ and $\chi_{||}$ separately for $T\geq T_C$, where no magnetization vector exists.

Within molecular-field theory, the longitudinal part of the susceptibility is (again for small $\vec{Q}$)

$$\chi_{||}(\vec{Q})=\frac{B}{Q^2+\kappa^2}\ , \tag{5}$$

which does not diverge as $\vec{Q}\to\vec{0}$ for $T\neq T_C$, where the inverse correlation length κ is finite. A more refined analysis,[10] which includes the effects of spin waves on the correlation function $\langle S^z(r)S^z(r')\rangle$, shows that in addition to a term like (5), $\chi_{||}(\vec{Q})$ also includes a term proportional to

$$G(\vec{Q})=\left[\frac{1}{Q^2+\kappa^2}\right]^2\frac{1}{Q}\ . \tag{6}$$

Expression (6) does diverge as $\vec{Q}\to\vec{0}$, but much less strongly than $\chi_\perp(\vec{Q})$ [Eq. (4)]. Furthermore, as T approaches the Curie temperature T_C, Eq. (5) represents the dominant component of $\chi_{||}(\vec{Q})$ at accessible values of Q. Indeed, after subtraction of the estimated contribution of $\chi_\perp$, the SANS spectra, shown in paper I, for $(Fe_{0.75}Mn_{0.25})_{75}P_{16}B_6Al_3$ with $T\lesssim T_C$ are very well described by the Lorentzian form (5).

While the static $\vec{Q}$-dependent susceptibilities $\chi_{||}(\vec{Q})$ and $\chi_\perp(\vec{Q})$ for Heisenberg ferromagnets are well understood, no universally accepted spectral weight functions exist. Three forms are commonly used for $F_\perp(\vec{Q},\omega)$: (i) a double Lorentzian, (ii) a damped harmonic oscillator, and (iii) an expression suggested by Halperin and Hohenberg.[11] For fixed $\vec{Q}$, these forms depend on two parameters which are essentially the frequency ω_0 and inverse lifetime Γ of a spin wave with wave vector $\vec{Q}$. If $\Gamma\ll\omega_0$, all three forms reduce to a pair of sharp peaks, centered at $\omega=\pm\omega_0$ and with half widths at half maximum (HWHM) of Γ. For $\omega_0\lesssim\Gamma$, the three forms are not identical and efforts to fit experimental data will yield different results for ω_0 and Γ depending upon the form used in the analysis.[5] It is well known that this ambiguity makes verification of dynamical scaling near an ordinary FM transition difficult.[12] There is even less theoretical guidance on the form of $F_\perp(\vec{Q},\omega)$ near the FM-SG crossover.

We now recapitulate the results of elementary spin-wave theory[9] for ω_0 and Γ. Firstly, in a purely exchange-coupled ferromagnet with Hamiltonian

$$H_0=-\sum_{n,m}J_{nm}\vec{S}_n\cdot\vec{S}_m\ , \tag{7}$$

spin waves at a given $\vec{Q}$ have an energy

$$E_{ex}(\vec{Q})=2S[J(0)-J(Q)]\ , \tag{8}$$

where

$$J(\vec{Q})=\sum_m J_{nm}\exp[i\vec{Q}\cdot(\vec{r}_n-\vec{r}_m)]\ . \tag{9}$$

$E_{ex}(\vec{Q})$ for small $\vec{Q}$ can be expanded as

$$E_{ex}(\vec{Q})=DQ^2+EQ^4+\cdots\ . \tag{10}$$

In cubic systems, D is an isotropic stiffness constant. At nonzero temperatures, the spin waves interact with each other, and D is reduced from its value at $T=0$ according to the well-known law

$$D(T)=D(0)(1-aT^{5/2}+\cdots)\ . \tag{11}$$

Also because they interact, the spin waves are damped, with an estimated inverse lifetime given by the formula[13]

$$\Gamma(Q)=\gamma_{eff}Q^4\ , \tag{12}$$

where

$$\gamma_{eff}=\Gamma_0T^2\ln^2[kT/E_{ex}(\vec{Q})]\ . \tag{13}$$

Hydrodynamic spin-wave theory[14] gives Eq. (12), but not the detailed form (13) for γ_{eff}. Equations (10)—(13) have been found to be consistent with data taken well below T_C for both crystalline and amorphous ferromagnets.[15]

Including dipolar interactions in addition to the exchange terms modifies the spin-wave dispersion relation Eq. (8). Assuming that the domains in the ferromagnet are needlelike and point parallel to the magnetization $\vec{M}$, the spin-wave energy becomes, for $4\pi g\mu_B|\vec{M}|\ll E_{ex}(\vec{Q})$,

$$\hbar\omega_0(\vec{Q})=E_{ex}(\vec{Q})+\sin^2\theta_{\vec{Q}}\,2\pi g\mu_B|\vec{M}|\ , \tag{14}$$

where $\theta_{\vec{Q}}$ is the angle formed between $\vec{Q}$ and $\vec{M}$. In a powder sample, or for randomly packed amorphous ribbons, as in our experiment, a constant $\vec{Q}$ inelastic scan measures the average of the transverse spectral weight

function over all directions of $\vec{M}$. The dipolar interactions thus lead both to a broadening of order $\pi g\mu_B M$ in the observed spin-wave spectra, and a shift $\Delta=(4\pi/3)g\mu_B M$ in the mean excitation energy. Thus, for the momentum transfer typically probed in neutron scattering experiments on polycrystalline and amorphous ferromagnets,[15] the observed spin-wave dispersion is described by the form

$$\hbar\omega_0=DQ^2+\Delta \ . \tag{15}$$

Δ is usually called the dipolar anisotropy gap, although, strictly speaking, $\hbar\omega_0(\vec{Q})$ vanishes linearly (rather than quadratically as in the purely exchange-coupled case) with $|\vec{Q}|$, unless $\vec{Q}||\vec{M}$. It is sometimes convenient to rewrite (15) as

$$\hbar\omega_0=D_{\rm eff}Q^2 \ , \tag{16}$$

where

$$D_{\rm eff}=\Delta Q^{-2}+D \ . \tag{17}$$

In general, there are two contributions to the longitudinal spectral weight function $F_{||}(\vec{Q},\omega)$. The first is due to spin diffusion and appears as a single peak centered at $\omega=0$. The second is derived from the coupling of longitudinal fluctuations to spin waves and consists of a pair of peaks centered at $\omega=\pm\omega_0$, where ω_0 is the spin-wave frequency. In ordinary ferromagnets[15] below T_C, the diffusive central peak has never been observed: The inelastic neutron scattering spectra only show two spin-wave peaks. This is in contrast to the situation for Heisenberg antiferromagnets, where a central peak is indeed present at temperatures close to, but below the Néel temperature.[16] Thus, for a system such as $(Fe_{1-x}Mn_x)_{75}P_{16}B_6Al_3$, with *mixed* ferromagnetic and antiferromagnetic interactions, there is no *a priori* reason to exclude a central peak from $F_{||}(\vec{Q},\omega)$.

We turn now to the Fourier transform $\tilde{S}^{\alpha\beta}(\vec{Q})$ of the static spin-spin correlation function introduced in Eq. (3):

$$\tilde{S}^{\alpha\beta}(\vec{Q})=\sum_{m,n}\exp[i\vec{Q}\cdot(\vec{r}_m-\vec{r}_n)]\langle S_m^{\alpha}(t=\infty)S_n^{\beta}(t=0)\rangle \ . \tag{18}$$

If the spins $\vec{S}_n$ are aligned ferromagnetically, for example along the z axis, $\tilde{S}^{\alpha\beta}(\vec{Q})$ vanishes except when $\alpha=\beta=z$, in which case it is directly proportional to the Fourier transform $\rho(\vec{Q})$ of the pair-correlation function for the magnetic ions:

$$\begin{aligned}\tilde{S}^{zz}(\vec{Q})&=|\langle S^z\rangle|^2\sum_{m,n}\exp[i\vec{Q}\cdot(\vec{r}_m-\vec{r}_n)]\\&=|\langle S^z\rangle|^2\rho(\vec{Q}) \ .\end{aligned} \tag{19}$$

For a crystalline system, $\rho(\vec{Q})$ is a sum of δ functions centered at reciprocal-lattice points and vanishes elsewhere. On the other hand, $\rho(\vec{Q})$ for an amorphous solid generally vanishes nowhere in reciprocal space. Therefore, in principle, $\tilde{S}^{\alpha\beta}(\vec{Q})$ will never be strictly zero for an amorphous ferromagnet below its Curie temperature. Because $\tilde{S}^{\alpha\beta}(\vec{Q})$ represents *static* spin correlations, the magnetic scattering must have a purely elastic component at all $\vec{Q}$. In practice, as we have seen for $(Fe_{0.80}Mn_{0.20})_{75}P_{16}B_6Al_3$ in paper I, this component is only observable in the vicinity of a maximum in $\rho(\vec{Q})$. The maximum is usually not far from where a Bragg peak for the corresponding crystalline material would occur. The measurements to be described below were performed for small $\vec{Q}$ ($|\vec{Q}|<0.1$ Å^{-1}), where $\rho(\vec{Q})$ is known, from our x-ray and neutron-diffraction work,[1] to be small.

A more interesting contribution to $\tilde{S}^{\alpha\beta}(\vec{Q})$ is derived from frozen fluctuations in the directions, rather than the positions, of the spins. The simplest way to produce such fluctuations is to impose a random field on the system. The magnetic Hamiltonian is then changed from H_0 [Eq. (7)] to

$$H=H_0+h\sum_n\hat{h}_n\cdot\vec{S}_n \ . \tag{20}$$

In (20), the random-field directions $\hat{h}$ ($|\hat{h}|=1$) at different sites are uncorrelated, i.e.,

$$[\hat{h}_n^{\alpha}\hat{h}_m^{\beta}]_c=\tfrac{1}{3}\delta_{nm}\delta^{\alpha\beta} \ , \tag{21}$$

where $[\ ]_c$ denotes the average over all possible random-field configurations.

If $h\gg|J_{nm}|$,

$$\langle\vec{S}_n\rangle_T=\hat{h}_n\left[\coth\frac{h}{kT}-\frac{kT}{h}\right]=\hat{h}_nL(h/kT) \ , \tag{22}$$

and from (21),

$$[\langle S_n^{\alpha}\rangle\langle S_m^{\beta}\rangle]_c=\tfrac{1}{3}\delta_{nm}\delta^{\alpha\beta}L^2(h/kT) \ , \tag{23}$$

which immediately implies that $\tilde{S}^{\alpha\beta}(\vec{Q})$ is both nonvanishing and $\vec{Q}$ independent. What happens when $h\lesssim|J_{nm}|$ is a subject of considerable current interest. For exchange-coupled Heisenberg systems in less than four dimensions, long-range ferro- or antiferromagnetic order is thought to be unstable with respect to infinitesimal h. Even at zero temperature, the δ-function Bragg peaks comprising $\tilde{S}^{\alpha\beta}(\vec{Q})$ are expected to become the sums of various powers of Lorentzians with finite widths.[17]

A spin glass with nonvanishing Edwards-Anderson order parameter $Q_{\rm EA}$ is another system which displays nonvanishing static spin fluctuations. Recall that the Hamiltonian here is given by Eq. (7), where the exchange, constants J_{nm} are randomly selected from some distribution.[18] The Edwards-Anderson order parameter $Q_{\rm EA}$ is precisely equal to the average of $\sum_{\alpha}\tilde{S}^{\alpha\alpha}(Q)$ over reciprocal space:[19]

$$\begin{aligned}Q_{\rm EA}&=\frac{1}{N}\sum_m\langle\vec{S}_m(0)\cdot\vec{S}_m(t=\infty)\rangle\\&=\frac{1}{N}\sum_{m,n}\frac{\int d^3Q\exp[i\vec{Q}\cdot(\vec{r}_n-\vec{r}_m)]}{\int d^3Q}\\&\qquad\times\langle\vec{S}_m(0)\cdot\vec{S}_n(t=\infty)\rangle\\&=\frac{\int d^3Q\sum_{\alpha}\tilde{S}^{\alpha\alpha}(\vec{Q})}{\int d^3Q} \ .\end{aligned} \tag{24}$$

Neutron scattering measurements of purely elastic magnetic scattering should therefore give Q_{EA} directly. Real experiments are characterized by finite energy resolution ΔE, and so all processes with relaxation times $\tau > \hbar/\Delta E$ will contribute to the nominally elastic scattering. The order parameter scattering in normal ferro- and antiferromagnets is easy to identify, since it is located at particular (discrete) reciprocal-lattice vectors, whereas in the canonical spin-glass it is *by definition* uniformly dispersed throughout reciprocal space and correspondingly less intense at any given $\vec{Q}$. Furthermore, as shown both by computer simulations[20] and real experiments,[21] spin-glasses display many excitations with extraordinarily low frequencies. Recent theoretical studies[22] have related these excitations to the difficulties encountered in previous analytic approaches to the spin-glass problem. The same studies have also emphasized that averages like (24) which involve $t \to \infty$, are not uniquely defined in the thermodynamic ($N \to \infty$) limit.

In spite of the problems mentioned above, neutron scattering has been a very useful tool for investigating the behavior of ordinary (nonreentrant) dilute spin-glasses, such as Cu-Mn. This is particularly true because of the large variety of available instruments, which have resolutions ΔE corresponding to time scales τ varying from 10^{-11} sec (standard triple-axis or time-of-flight spectrometers) to 10^{-8} sec (spin-echo spectrometer). Murani and Heidemann[19] carried out a detailed study of the "elastic" signal from the classical SG alloy, CuMn, for which the ac susceptibility has its characteristic cusp at $T_g^{ac} = 39$ K. This signal was temperature independent for T larger than an apparent freezing temperature T_g, while for $T < T_g$ it increased monotonically. As ΔE was reduced from 230 μeV to 1.5 μeV, T_g fell from a value of roughly twice T_g^{ac} to only 20% more than T_g^{ac}. We are not aware of measurements performed with similarly good resolution (1.5 μeV) in the SG regimes of more concentrated alloys with or without higher-temperature FM states. Of course, RSG systems are even more suited for neutron scattering studies than the classical SG alloys. This is because the order parameter scattering will be relatively more intense in certain special regions of reciprocal space, i.e., near Bragg peaks and the forward direction.

III. EXPERIMENTAL

A. Samples and cryostats

The $(Fe_{1-x}Mn_x)_{75}P_{16}B_6Al_3$ samples used were the same as those described in paper I. Table I gives a list of these samples and the corresponding magnetic transition temperatures, established from our previous neutron scattering measurements.[1] Table I also shows the transition temperatures obtained from bulk susceptibility data for samples with the same nominal concentrations, i.e., ratios of starting materials. The discrepancies between the neutron and bulk results are probably due to differences in the real concentrations. On the ferromagnetic side of the phase diagram, the Curie temperature is probably the best indicator of the true concentration. The amorphous ribbons were packed into $\frac{3}{8}$-in.-diam tubes, masked with cadmium at either end to leave a sample volume with 1-in. height matched to that of the incident neutron beam. The sample tubes were mounted in closed-cycle Displex cryostats whose temperatures T could be controlled to better than 0.1 K between 10 and 325 K. To study behavior at lower temperatures, we installed the tubes in He^4 flow Dewars which allowed temperatures as low as 5 K to be reached. Investigations of magnetic field effects were carried out using a split-coil superconducting magnet and a conventional electromagnet.

B. Neutron scattering technique

Our neutron scattering technique was similar to that employed in previous studies of the spin dynamics of amorphous ferromagnets.[15] Owing to the lack of translational order in such materials, the measurements were all carried out around the (000) "Bragg peak," i.e., near the forward direction.

Neutron scattering measurements were performed on various spectrometers at the Brookhaven National Labo-

TABLE I. Magnetic properties of $(Fe_{1-x}Mn_x)_{75}P_{16}B_6Al_3$ alloys.

		T_c (K)			T_g (K)			Spin waves[d] T_{max}	D_{max}	Δ
x[a]	SANS[b]	BULK[2]	BULK[3]	SANS[b]	IENS[c]	BULK[2]	BULK[3]	(K)	(meV Å^2)	(μeV)
0.35[e]		42±2		42±10		42	42			
0.30	143±2	107±2	114	20±3	80	31±2	54	125	8.5±1.0[f]	
0.25	221±1				65			145	21.0±0.7	16±4
0.20	340±5[g]	293±4	280		30	14±2	34	150	47.1±0.7	21±2

[a]Nominal concentrations, given by ratios between starting materials.
[b]Small-angle neutron scattering results for $Q = 0.02$ Å^{-1}, reported in paper I.
[c]Inelastic neutron scattering, reported in present paper. These temperatures are the highest temperatures in the regime where no resolvable spin-wave peaks were found.
[d]Spin-wave stiffness D_{max} and anisotropy gap Δ at temperature T_{max} where spin-wave energies are highest.
[e]Bulk measurements are reported for $x = 0.34$.
[f]Measurement of D_{eff} for $Q = 0.075$ Å^{-1}.
[g]Measured on a conventional triple-axis spectrometer for $Q = 0.03$ Å^{-1}.

ratory High Flux Beam Reactor. Pyrolytic graphite crystals, set for the (002) reflection, were used as monochromators and analyzers in all of our experiments. The incident neutrons had energies $E_i < 5$ meV; to eliminate higher-order contamination, they were passed through a liquid-nitrogen-cooled beryllium filter.

Much of the data was collected at the cold neutron source of the HFBR. The spectrometer here is equipped with a double crystal monochromator which allows incident energies E_i as low as 2.3 meV to be reached. Three sets of collimating blades—one before the first crystal, one between the two crystals, and one after the second crystal—define the angular divergence of the neutron beam impinging on the sample. The analyzer assembly for this spectrometer is identical to that for standard triple-axis spectrometers: It consists of one pyrolytic graphite crystal mounted on a motorized goniometer, and entrance and exit collimators. Inelastic scans are performed by scanning E_i while keeping the final energy E_f fixed. We varied E_f and the collimator configuration to obtain different combinations of resolution and intensity. The resulting values of the energy resolution ΔE were between 0.025 and 0.060 meV, numbers which represent full widths at half maximum (FWHM) of the inelastic spectra that would be collected for a purely incoherent ($\vec{Q}$-independent) elastic scatterer.

Ordinary triple-axis spectrometers with single-pass monochromators were used for our other measurements. We carried out constant $\vec{Q}$ energy scans by varying the final energy E_f while keeping E_i fixed at either 3.5 or 4.5 meV. The corresponding energy resolutions ΔE were between 0.05 and 0.10 meV (FWHM).

C. Background

There are two different types of background signals in inelastic neutron scattering measurements. The first is derived from ambient fast neutrons in the experimental area and is therefore independent of energy and momentum transfer. To reduce this background, considerable efforts were made to shield our apparatus from neighboring beam ports at the HFBR. We have established the background level with the neutron shutter at our experimental station open, and both the sample and cryostat in place, by measuring the scattering at relatively large momentum and energy transfer (e.g., $Q=0.1$ Å^{-1} and $E_f-E_i=0.5$ meV). True inelastic scattering from our sample was reduced by going to the lowest temperature (5 or 10 K) accessible with the cryostat in question. The resulting background count rates were between 1 and 2.5 counts per minute.

The second type of background is a purely elastic signal which is ordinarily due to incoherent isotopic scattering from the sample and scattering from the sample holder and cryostat. In our experiment, which was performed near the forward direction, the direct beam is another possible background source. Furthermore, in amorphous systems such as $(Fe_{1-x}Mn_x)_{75}P_{16}B_6Al_3$, the structure function $\rho(\vec{Q})$ is nonvanishing throughout reciprocal space and therefore contributes to the nonmagnetic elastic signal. We emphasize that the various constituents of the elastic background are essentially temperature independent but can be strongly Q dependent. For normal ferromagnets, the most common procedure[14,15] is to identify the elastic background $B(\vec{Q})$ with the total elastic scattering observed within the ferromagnetic phase, where the spin-wave peaks are at several half-widths distance from the elastic position. This procedure is inherently unreliable for random ferromagnets. Both in principle, as discussed in Sec. II, and in practice, as described below, such systems can exhibit considerable quasielastic magnetic scattering in addition to well-resolved spin-wave peaks. Nevertheless, the standard procedure, which entails measuring $B(\vec{Q})$ when the spin-wave stiffness is highest, does give upper bounds on $B(\vec{Q})$. For $(Fe_{1-x}Mn_x)_{75}P_{16}B_6Al_3$, these bounds are sufficiently low so that more precise knowledge of the elastic background would not change our conclusions about the magnetic scattering. This will become evident when we present our data in Sec. IV.

D. Data analysis

For the purposes of our data analysis, we assume a cross section consisting of a transverse (spin-wave) relaxation spectrum and a quasielastic component. From Eqs. (1) and (3),

$$\frac{\partial^2\sigma}{\partial\Omega\,\partial\omega}=c\frac{|\vec{k}_f|}{|\vec{k}_i|}\left[\frac{\hbar\omega/kT}{1-\exp(-\hbar\omega/kT)}\chi_0^{-1}\chi_\perp(\vec{Q})F_\perp(\vec{Q},\omega)+[\tilde{S}(\vec{Q})+B(\vec{Q})]\delta(\omega)\right]. \tag{25}$$

In Eq. (25), c is a constant, independent of $\vec{Q}$, ω, and T. Since our measurements are performed over a very small range in $\vec{Q}$ ($|\vec{Q}|<0.1$ Å^{-1}), we neglect the $\vec{Q}$-dependent ionic form factor $|f(\vec{Q})|^2$ which appears in Eq. (1). The various terms in Eq. (25) have the same meaning as in Sec. II. Recall that the transverse susceptibility $\chi_\perp(\vec{Q})=\chi_0 A_s Q^{-2}$ [Eq. (4)]. We have chosen the Lorentzian form for the spectral function,

$$F_\perp(\vec{Q},\omega)=\frac{1}{2\pi}\left[\frac{\Gamma}{(\omega-\omega_0)^2+\Gamma^2}+\frac{\Gamma}{(\omega+\omega_0)^2+\Gamma^2}\right], \tag{26}$$

because it is the form most frequently used in the study of normal ferromagnets.[15] Shapiro and co-workers have also used this form in their extensive survey of the spin dynamics of Fe_xCr_{1-x}.[4] The spin waves were assumed to obey the quadratic dispersion law (16). For each $\vec{Q}$, we varried the effective spin-wave stiffness $D_{\rm eff}$ to obtain the best fit, as described below.

For our analysis of the $x=0.25$ and 0.30 data, the spin-wave damping coefficient Γ was a $\vec{Q}$-independent quantity in each of our fits. For $x=0.20$, we assumed that Γ behaved as in the hydrodynamic theory of spin waves [Eq. (12)] and varied $\gamma_{\rm eff}$ (for each spectrum) instead.

The term $\tilde{S}(\vec{Q})+B(\vec{Q})$ in Eq. (25) includes contributions from (i) the elastic nonmagnetic background $B(\vec{Q})$, (ii) "frozen" spin clusters, and (iii) any part of the magnet-

ic response peaked at $\omega=0$. The reader should refer to Secs. III C and II for extensive discussions of each of these contributions. Because we have no *a priori* knowledge of how $\tilde{S}(\vec{Q})+B(\vec{Q})$ varies with $\vec{Q}$ and T, we allowed it to vary freely in most of our fits. After some experimentation, we selected the trial form

$$\tilde{S}(\vec{Q})+B(\vec{Q})=A_G/Q^2 . \tag{27}$$

Note that if $\hbar\omega_0$ and $\Gamma \ll kT$,

$$(A_G+A_S)Q^{-2}=\int_{-\infty}^{\infty} d\omega\{\chi_0^{-1}\chi_\perp(\vec{Q})F_\perp(\vec{Q},\omega) +[\tilde{S}(\vec{Q})+B(\vec{Q})]\delta(\omega)\}$$

$$\approx \int \frac{\partial^2\sigma}{\partial\Omega\,\partial\omega}d\omega \tag{28}$$

is what would be measured in a quasielastic scattering experiment.

The cross section (25) cannot be directly compared to the experimental data because it has not been corrected for the finite resolution of the spectrometer. Resolution effects are particularly important in experiments such as ours where the excitation energies are small and the nominal momentum transfer $\vec{Q}$ has a magnitude comparable to the vertical (out of the scattering plane) resolution ΔQ_z of the spectrometer. As discussed before, in the context of measurements of spin waves in amorphous ferromagnets,[15] the generally poor ΔQ_z (>0.05 Å^{-1} FWHM) of ordinary triple-axis spectrometers will cause the spin-wave peak observed at a certain $\vec{Q}=(Q_x,0,0)$ to appear at an energy $E \gtrsim \hbar\omega_0(\vec{Q})$. Fortunately, the resolution function is well described by a four-dimensional Gaussian in $\vec{Q}$ and ω. The covariance matrix and multiplicative prefactor for the Gaussian can be calculated analytically.[23] The input parameters from this calculation include the acceptance angles of the collimators, the energies of the incident and scattered neutrons, and the nominal momentum transfer for which the spectrometer is set. The theoretical form that we actually compare to the data is then the convolution of Eq. (25) with the Gaussian resolution function. The convolution is performed using a 5000- to 10000-point Monte Carlo integration routine.

In our nonlinear least-squares-fitting procedure, the mean-square deviation of the computed cross section from the data is minimized with respect to the four parameters A_G, A_S, $D_{\rm eff}$, and Γ (or $\gamma_{\rm eff}$). We do this independently for each constant $\vec{Q}$ spectrum, which allows us to check if the $\vec{Q}$ dependence of the theoretical cross section is consistent with the data.

IV. RESULTS AND ANALYSIS

A. $x=0.35$

Recall that our SANS measurements for this concentration,[1] as well as recent bulk susceptibility measurements,[3] give no evidence for ferromagnetism in this compound. However, a spin-glass transition is thought to occur at $T=T_g^{\rm ac}=42$ K, which is also where the SANS signal exhibits a broad maximum. In Fig. 2, we show a temperature scan taken on a triple-axis spectrometer set for constant Q and zero-energy transfer. The data, which account only for scattering within the narrow window of energy transfers given by the spectrometer resolution (0.05 meV FWHM), are very similar to those obtained in our quasielastic SANS measurements. Figure 3 shows

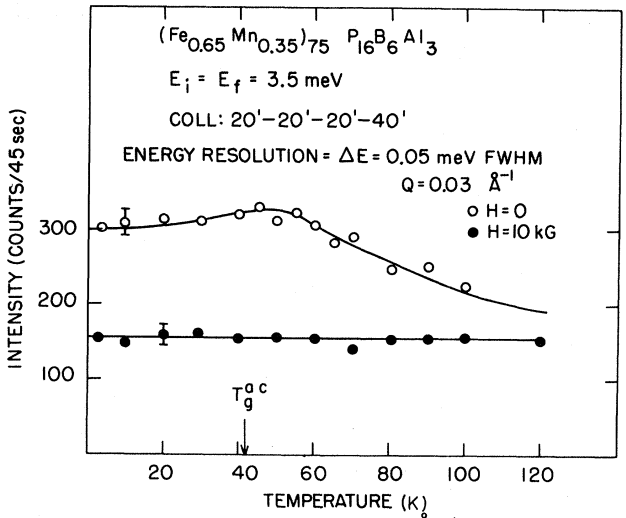

FIG. 2. Elastic intensity at $Q=0.03$ Å^{-1} as a function of temperature. The 10-kG field was applied perpendicular to the horizontal scattering plane.

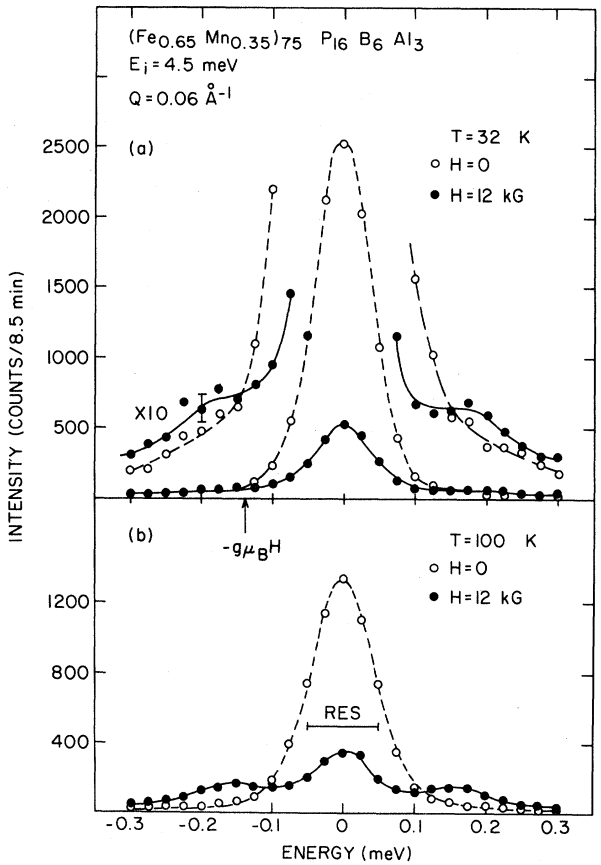

FIG. 3. Inelastic spectra for the $x=0.35$ sample at $T=32$ and 100 K. The 12-kG field was applied in the scattering plane such that at $E=0$, it was nearly perpendicular to Q. Lines through the data points are guides to the eye. These data have not been corrected for background.

constant-Q energy scans for one temperature well above ($T=100$ K) and another well below ($T=32$ K) the anomaly at $T_g \simeq 50$ K. The dominant feature of our spectra is a resolution-limited peak centered at $E=0$; the sole identifiable difference between the $T=100$ and $T=32$ K results is an increase in the amplitude of this peak.

We have also carried out a preliminary study of the magnetic field dependence of the scattering. In a normal ferromagnet, a nonzero field H shifts the spin wave dispersion curve Eq. (9) to higher energies by an amount $g\mu_B H$, and increases Bragg scattering at the expense of diffuse scattering. Note that $g\mu_B H$ is simply the Larmor precession frequency for a free spin. For the purposes of our discussion here, we always take $g=2$, which is the g factor for an electron.

The solid circles in Fig. 2 represent measurements performed while warming the sample in a 10-kOe field applied perpendicular to the scattering plane. It is apparent that this relatively small field ($g\mu_B H=0.12$ meV$=1.35$ K) completely suppresses the temperature dependence of the scattering found for $H=0$. Figure 3 shows the influence of a 12-kG field on the inelastic spectra. In this case H was in the scattering plane and nearly perpendicular to $\vec{Q}$ at zero-energy transfer. For both $T=32$ and 100 K, the field reduces the quasielastic scattering substantially. Furthermore, inelastic sidebands, centered at ± 0.14 meV$=\pm g\mu_B H$, appear. Spectra collected for other $\vec{Q}$ and $\vec{H}$ are similar, and the positions of the inelastic sidebands deviate negligibly from the free spin values $\pm g\mu_B H$.

B. $x=0.30$

This composition is on the ferromagnetic side of the SG-PM-FM multicritical point, and according to our SANS measurements, has a Curie temperature $T_C=143$ K. Figure 4(a) displays energy scans taken at 125 K for $Q=0.060$ and 0.075 Å^{-1}. The $Q=0.075$ Å^{-1} spectrum (open circles) shows inelastic sidebands, in addition to a central peak. As Q is reduced to 0.06 Å^{-1} (solid circles), these sidebands move to lower-energy transfer and become more difficult to resolve. The spectra thus constitute evidence for spin waves in this material, and are indeed well described by the cross section (25) with $D_{\text{eff}}=8.5$ meV Å^2, folded with the instrumental resolution function.

In Fig. 4(b), we show inelastic scans collected for $Q=0.06$ Å^{-1} at 60 and 10 K, temperatures which are, respectively, above and below the spin-glass freezing temperature $T_g=54$ K found from macroscopic measurements.[3] As for the $x=0.35$ material, the dominant feature of both of these spectra is a resolution-limited peak centered at $E=0$. (Note that the energy resolution is more than three times better in Fig. 4 than in Fig. 3.) Even so, discernible inelastic scattering, absent at 10 K, is clearly present at 60 K, as evidenced by the temperature-dependent wings in the spectra. In view of the large quasielastic peak and the small D of this material, interpretation of the inelastic scattering here is difficult. Fortunately, the alloys with higher iron content exhibit qualitatively similar behavior which is more amenable to analysis.

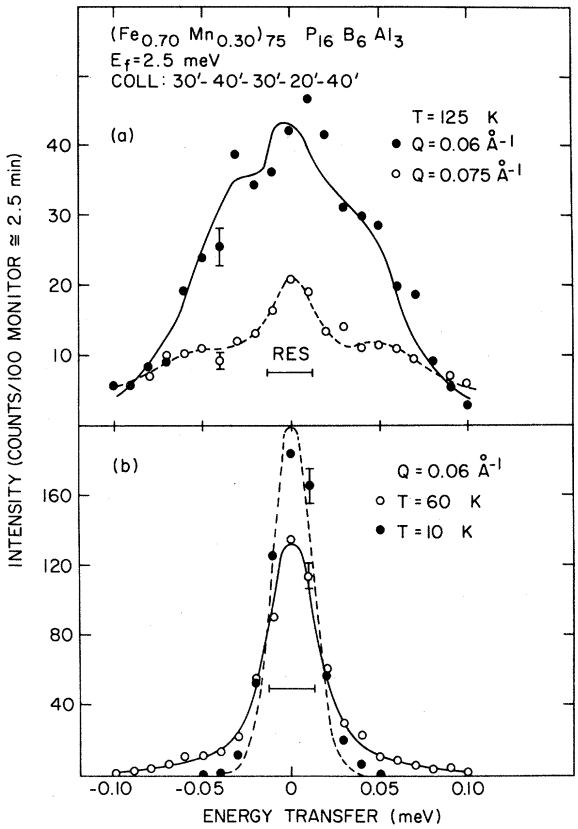

FIG. 4. Inelastic spectra for $x=0.30$. A constant background (1.8 counts/min), independent of energy and momentum transfer, has been subtracted from the raw data to yield these spectra. Lines for $T=125$ and 60 K represent computed cross sections resulting from four-parameter fits described in text. Dashed line for $T=10$ K [frame (b)] is a resolution-limited Gaussian. Note the narrow energy scale and resolution window (25 μeV FWHM).

C. $x=0.25$

The Curie temperature for this alloy is $T_C=221$ K. Figure 5 shows the evolution of the inelastic scattering at $Q=0.07$ Å^{-1} in the ferromagnetic phase. There are clearly resolvable spin-wave peaks in addition to a relatively weak quasielastic peak. With decreasing T, the spin-wave peaks first move towards higher energies, as they should in a normal ferromagnet. However, below 100 K, they return to lower energies. At the same time, the scattering at $E=0$ grows, and for $T<65$ K, there are no resolvable spin-wave peaks. Figure 6 shows spectra collected at $T=50$ and 10 K. These data are very similar to those given in Fig. 4(b) for $x=0.30$: at the higher temperature, considerable true inelastic scattering is still observed. Also, as T is lowered to 10 K, the Gaussian resolution function (dashed line) adequately accounts for the scattering profile.

We have analyzed our data following the procedures described in Sec. III. The solid lines in Figs. 5 and 6 represent the computed cross section for the final values of the parameters D_{eff}, A_S, Γ, and A_G given by our data fitting routine. Figure 7(a) shows the Q dependence of the

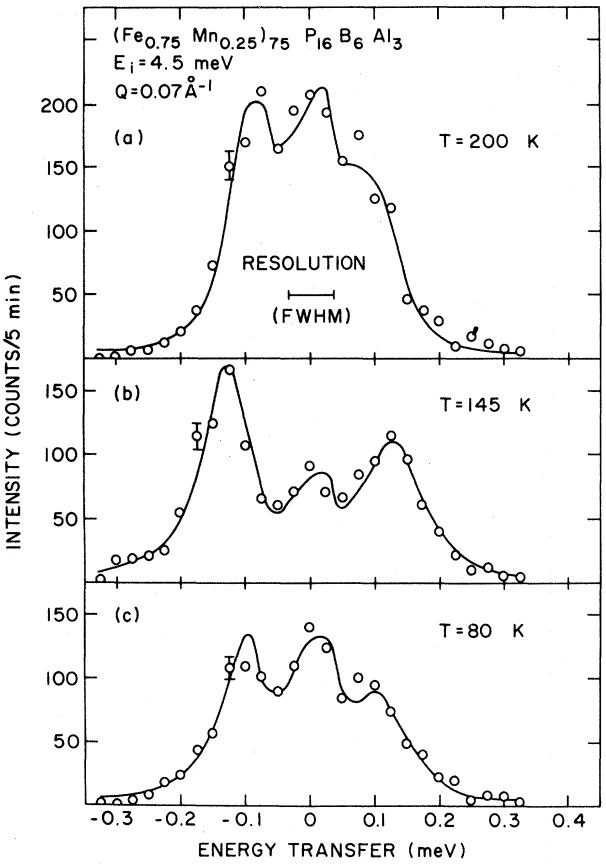

FIG. 5. Temperature dependence of inelastic spectra in ferromagnetic regime for $x=0.25$. Solid lines represent computed cross section resulting from four-parameter fits described in text. These spectra have been corrected for a flat background of 1.5 counts/min.

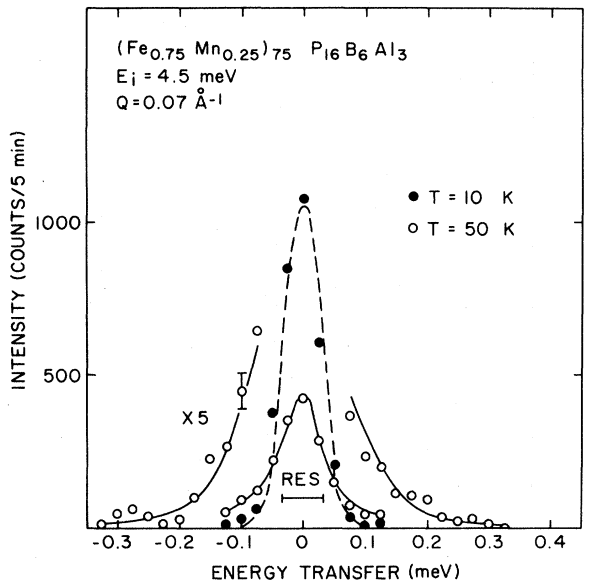

FIG. 6. Low-temperature spectra for $x=0.25$. These spectra have been corrected for a flat background of 1.5 counts/min. Solid line represents computed cross section resulting from four-parameter fit described in text. Dashed line is a resolution-limited elastic peak.

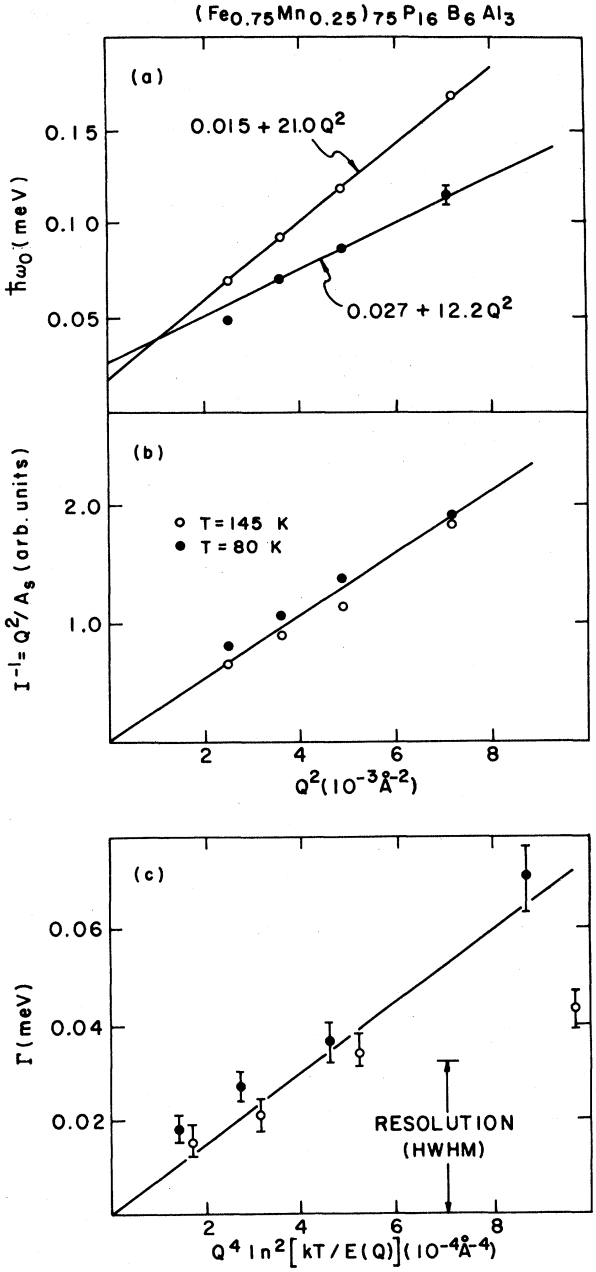

FIG. 7. Q dependence of parameters describing spectra for $x=0.25$. The solid lines in (a) represent the results of least-squares fits of $\hbar\omega_0(Q)$ to the form $\Delta+DQ^2$. The solid lines in (b) and (c) have been drawn as guides to the eye.

spin-wave energy $\hbar\omega_0(Q)=D_{\text{eff}}Q^2$ at $T=145$ and 80 K. The standard form (17) is sufficient to describe $\hbar\omega_0(Q)$ at all temperatures where the spin-wave peaks are resolvable.

We present our results for the integrated spin-wave intensity in the manner used to present our SANS data in paper I. Namely, we plot the inverse intensity $I^{-1}(Q)=Q^2/A_s$ against Q^2, as shown in Fig. 7(b) for $T=145$ and 80 K. In agreement with simple spin-wave theory, which predicts that $I(Q)\sim\chi_\perp(Q)\sim Q^{-2}$, we see that the data points fall on a straight line passing through the origin.

Simple spin-wave theory (see Sec. II) also predicts that

the damping Γ should obey Eq. (12). Accordingly, we have plotted, in Fig. 7(c) the values of Γ, given by our fits, against $Q^4\ln^2[kT/\hbar\omega_0(Q)]$. While our results are consistent with Eq. (12), they do not exclude other forms for the Q dependence of the damping.

We now turn to the temperature dependence of $D_{\rm eff}$, A_S, A_G, and A_S+A_G, shown in Fig. 8 for $Q=0.07$ Å^{-1}. Recall [see Eq. (28)] that for $\hbar\omega_0 \ll kT$ and $\Gamma \ll kT$, A_G+A_S corresponds to what is measured in a quasielastic scattering experiment, such as our SANS study of paper I. To obtain the results reproduced in Fig. 8, the four parameters A_S, A_G, Γ, and $D_{\rm eff}$ have been allowed to vary freely for all $T>10$ K. As pointed out above, there is no discernible inelastic scattering at 10 K (see Fig. 6), so here we set the spin-wave amplitude $A_S=0$ and varied only A_G to obtain the best fit.

The results shown in Fig. 8 have several important features. Firstly, as T is reduced from T_C, the spin-wave stiffness $D_{\rm eff}$ increases while the integrated spin-wave intensity A_S falls roughly in proportion to T. This of course is the behavior associated with a normal ferromagnet. At $T=145$ K, $D_{\rm eff}$ reaches its maximum value of 23 meV Å^2, after which it begins to decrease with decreasing temperature. Concomitantly, A_S drops much more slowly than it would in an ordinary ferromagnet where $A_S \sim T$. For $T<70$ K, the energy $\hbar\omega_0=D_{\rm eff}Q^2$ becomes comparable to both the inverse lifetime of the spin-wave excitation and the spectrometer resolution. Consequently, the results in this temperature range should only be interpreted as parametrizations of the data by the form defined in Eqs. (25)—(27). Even so, it is interesting to note that $D_{\rm eff}$ does not vary significantly with $T<65$ K. Furthermore, the integrated inelastic intensity, given by A_S, decreases again roughly in proportion to T. On the other hand, the elastic component A_G increases by an order of magnitude as T is lowered from 80 to 10 K. Consequently, the large upswing, which characterizes both the integrated intensity A_G+A_S in Fig. 6 and our quasielastic SANS data, described in paper I, is due to scattering which is elastic on the scale of our 65 μeV (FWHM) experimental resolution.

For this concentration, we have performed a brief survey of the inelastic scattering for $T>T_C=221$ K. Figure 9 shows spectra collected at $T=325$ K. These spectra broaden as Q is increased, which is suggestive of ordinary paramagnetic spin diffusion. To analyze the data, we have used the form

$$\frac{\partial^2\sigma}{\partial\Omega\,\partial\omega}=\frac{|\vec{k}_f|}{|\vec{k}_i|}[AF(\vec{Q},\omega)+B\delta(\omega)] \tag{29}$$

instead of Eq. (25). The spectral function $F(\vec{Q},\omega)$ is the Lorentzian given by the simple theory of spin diffusion, i.e.,

$$F(\vec{Q},\omega)=\frac{\Gamma}{\pi}\frac{1}{\Gamma^2+\omega^2} \tag{30}$$

with

$$\Gamma=\Lambda Q^2\,. \tag{31}$$

In our fits, we have allowed Λ, A, and the elastic background amplitude B to vary freely. Apart from our choice of the cross section (29), the resolution and background corrections, and the fitting procedure itself are exactly as described in Sec. III D. The solid lines in Fig. 9 represent

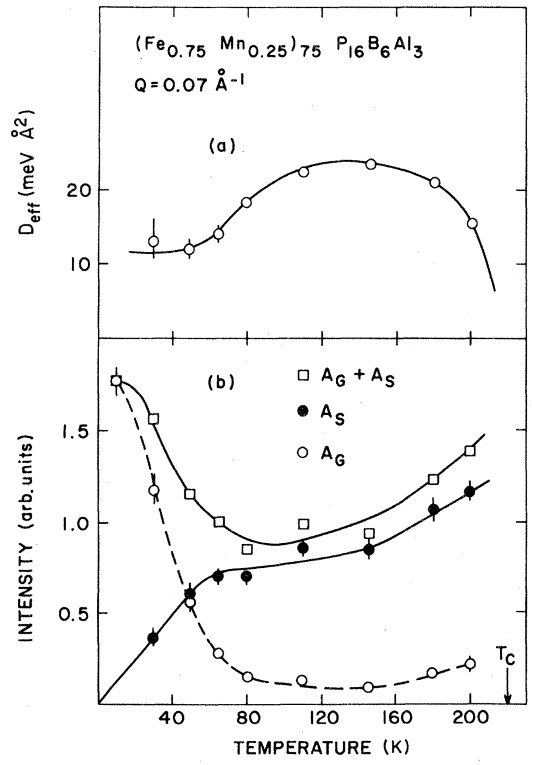

FIG. 8. Temperature dependence of fitting parameters $D_{\rm eff}$, A_S, and A_G for $x=0.25$

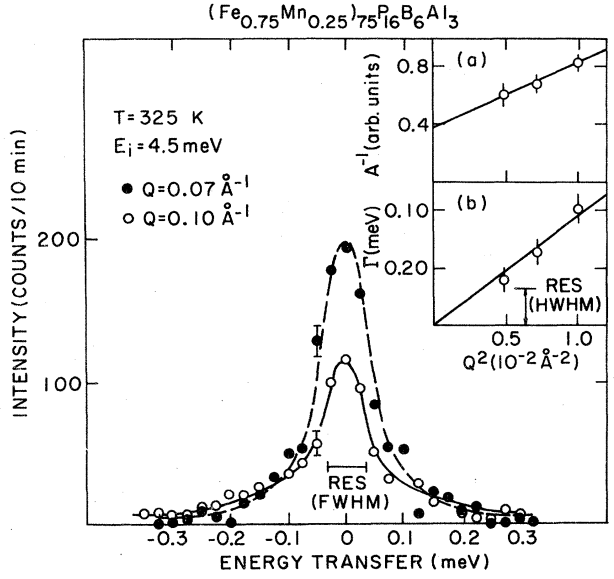

FIG. 9. Inelastic spectra in paramagnetic phase for $x=0.25$. These spectra have been corrected for a flat background 1.5 counts/min. Solid lines represent calculated intensity based on fits described in text. Inset shows fitted Lorentzian inverse amplitude A^{-1} and half width Γ plotted against Q^2.

the resulting theoretical spectra. Gratifyingly, the Lorentzian half-width Γ, shown in inset (b) of Fig. 9, rises with Q in a manner consistent with Eq. (31). The diffusion constant $\Lambda \simeq 10$ meV Å^2, which is comparable to the spin-wave stiffness constants D found below T_C. The inverse amplitude A^{-1}, shown in inset (a), also increases with Q, as it should for ferromagnetic critical scattering.

D. $x=0.20$

This is the most iron-rich and consequently the most ferromagnetic material that we have studied. Even so, the ac susceptibility measurements[3] indicate a spin-glass transition at $T_g \simeq 34$ K. The Curie temperature $T_C \simeq 342 \pm 5$ K, which we find from a survey of the critical scattering at $Q=0.03$ Å^{-1}, is higher than the values of 280–293 K given by bulk measurements.[2,3] Again, this probably follows from slight differences among the Mn concentrations of the samples studied.

Figure 10 shows energy scans taken at $Q=0.06$ Å^{-1} for various temperatures below T_C. Well-resolved spin-wave peaks are apparent in all but the lowest temperature (5 K) data. As for $x=0.25$, the spin-wave energy first increases, and subsequently decreases with decreasing T. However, the excitations here are sufficiently sharp and energetic on the scale of the experimental resolution that we can identify certain new features from direct inspection of the data. Notably, comparison of Figs. 10(b) and 10(c) shows that in addition to spin-wave softening, the quasielastic peak intensity independently undergoes a twofold increase. This of course justifies the use in our analysis of the nonstandard form for $\partial^2\sigma/\partial\Omega\,\partial\omega$, Eq. (25), which includes a peak at $\hbar\omega=0$ in addition to spin-wave sidebands at $\hbar\omega_0=\pm D_{\rm eff}Q^2$.

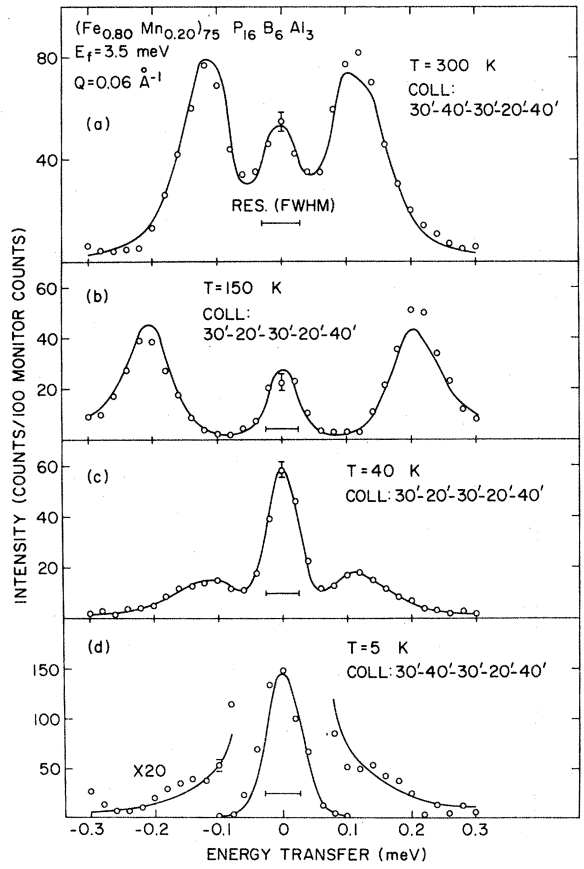

FIG. 10. Evolution with temperature of inelastic spectra for $Q=0.06$ Å^{-1} and $x=0.20$. Corrections have been made for a flat (Q- and E-independent) background. 100 monitor counters correspond to counting times of roughly 30 sec for (a), (c), and (d), and 1 min for (b). Solid lines represent the results of fits to the data.

In Fig. 11 we display the low-temperature evolution of the $Q=0.07$-Å^{-1} spectrum. Note that the spin-wave peaks cease to be resolvable between 35 and 20 K. Another important point is that the range of energy transfers over which inelastic scattering exists does not shrink noticeably with $T<35$ K. This suggests that as the spin-glass regime is entered, the effective stiffness does not vanish. Instead, the spin waves become highly damped.

Figure 12 shows inelastic scans for several $\vec{Q}$ at $T=5$ K. The spectra clearly become wider as $\vec{Q}$ is increased, which demonstrates the dispersive nature of the thermal fluctuations. We emphasize that the energy scale for these fluctuations in the spin-glass regime is similar to the spin-wave energy (at comparable $\vec{Q}$) for the lowest temperature (35 K) in the ferromagnetic regime.

The solid lines in Figs. 10–12 represent the results of fitting the data to the theoretical cross section (25). Figure 13 shows the $\vec{Q}$ dependence of $D_{\rm eff}Q^2$ and $\gamma_{\rm eff}Q^4$ at two various temperatures in the ferromagnetic regime. For fixed T, elementary spin-wave theory gives an excellent description of these data. Notably, the spin-wave energy $\hbar\omega_0(\vec{Q})=D_{\rm eff}Q^2$ obeys the dispersion law, Eq. (15). Furthermore, the damping $\Gamma=\gamma_{\rm eff}Q^4$ increases with Q in a manner consistent with Eq. (12). Finally, at each T, the spin-wave amplitude A_S (not shown) is independent of Q, to within experimental error. Consequently, the integrated inelastic intensity $A_S Q^{-2}$ follows the familiar Q^{-2} law.

In Fig. 14, we show the $\vec{Q}$ dependence of the results

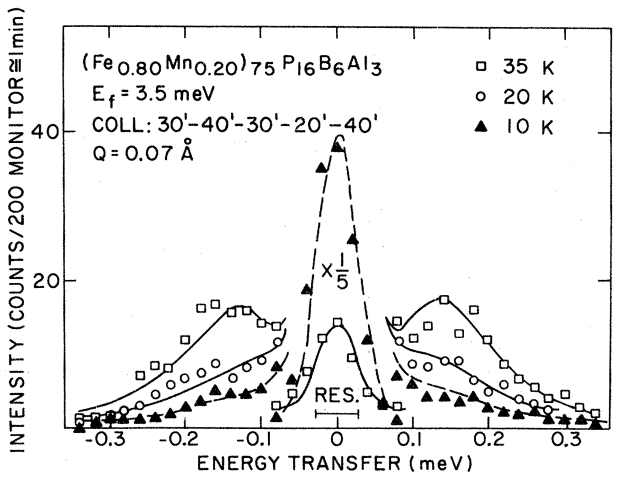

FIG. 11. Low-temperature evolution of $Q=0.07$ Å^{-1} spectrum, corrected for a flat background of 2.4 counts/min. Solid lines represent the computed cross section resulting from the fits described in the text.

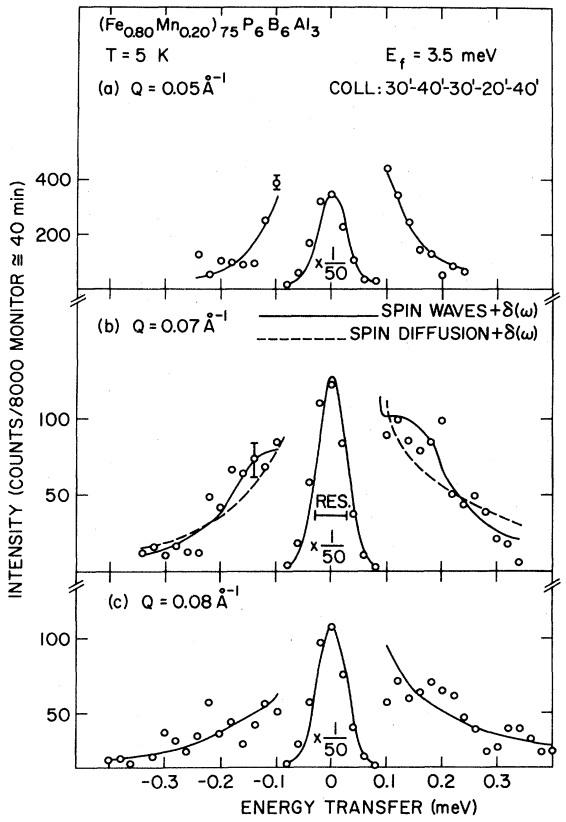

FIG. 12. Evolution with Q of spectra collected at $T=5$ K for $x=0.20$. The background signal subtracted is 2.4 counts/min. Solid lines represent the computed cross section resulting from the fits to Eq. (25) with D_{eff} allowed to vary freely. Dashed line in (b) corresponds to fit with D_{eff} fixed at zero.

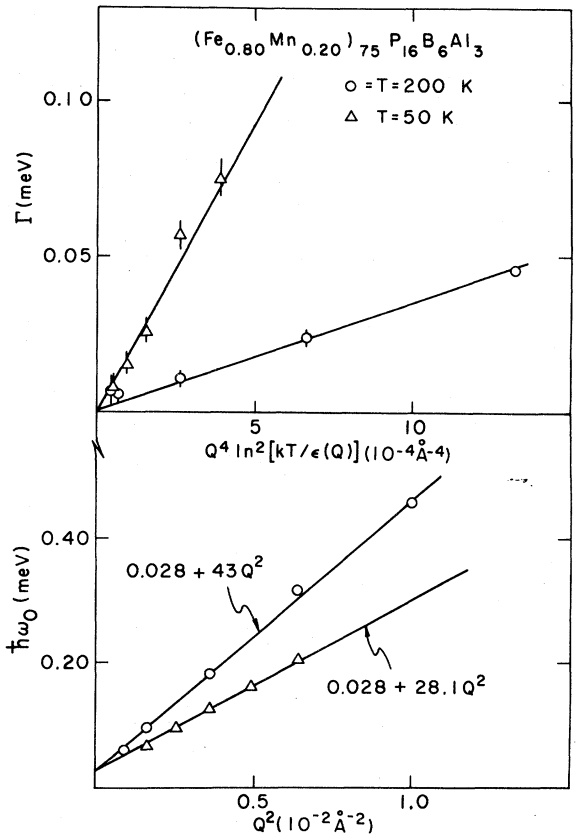

FIG. 13. Q dependence of parameters describing spin-wave spectra in ferromagnetic regime for $x=0.20$.

from our fits to data collected near and below the crossover temperature $T_g \approx 30$ K. Even though no resolvable spin-wave peaks exist for $T < T_g$, spin-wave theory is consistent with these results, which must only be regarded as parametrizations of the data. Interestingly, the spin-wave damping and stiffness parameters do not change significantly below T_g, while A_S scales in roughly linear fashion with T. In the range of experimentally accessible momentum transfers, the dynamics in the spin-glass (SG) and lower-temperature ferromagnetic regimes differ primarily because of the larger damping in the SG regime.

The quasielastic scattering increasingly dominates the spectra as T approaches zero. Figure 15 shows the Q dependence of the amplitude factor A_G. At temperatures above 30 K, we find that A_G is independent of $\vec{Q}$, so that the inelastic and quasielastic scattering intensities both obey a Q^{-2} law *over the range of accessible* $\vec{Q}$. For $T<30$ K, deviations from this law appear and the decay of the quasielastic intensity $A_G Q^{-2}$ is better described by a power law $Q^{-\alpha}$ with $\alpha > 2$. However, the statistical errors are such that $A_G = c$, where c is a $\vec{Q}$-independent constant, is not excluded as a possible interpretation of the data.

To assure ourselves of the significance of the above results, we have fitted some of the low-temperature spectra to Eq. (25) with D_{eff} held at zero. In this case, only A_G, A_S, and γ_{eff} were treated as free parameters. Note also that $F_\perp(\vec{Q},\omega)$ becomes a single Lorentzian, centered at $\omega=0$ and with half-width $\gamma_{\text{eff}}Q^4$. The dashed line in Fig. 12(b) indicates the computed cross section obtained from this procedure for $Q=0.07$ Å^{-1} and $T=5$ K. Note that the data are in somewhat better agreement with the solid curve, obtained from a fit where D_{eff} was allowed to vary. Thus, the use of D_{eff} as a free parameter is justified even at the lowest temperature studied.

To summarize our measurements on the $x=0.20$ sample, we show in Figs. 16 and 17 the temperature dependence of the four fitting parameters for $Q=0.06$ Å^{-1}. These results are qualitatively very similar to those shown in Fig. 8 for $x=0.25$. However, the energy scale, as measured by the maximum stiffness $D_{\text{eff}}=54$ meV Å^2 at $T=150$ K, is more than twice that for $x=0.25$. As the temperature is reduced from 150 to 50 K, the principal effects are a reduction in D_{eff} and corresponding increases in A_S/T and Γ. Below 50 K, there is large growth in the quasielastic scattering amplitude, and this accounts for the upswing in the integrated intensity A_G+A_S. For $T<30$ K, the spin-wave peaks become very broad. Nonetheless, the fitted value for D_{eff} remains constant to within statistical errors which increase considerably with decreasing T. Furthermore, A_S now decreases towards zero linearly with T. A_G continues to rise sharply, and exceeds A_S for $T<25$ K.

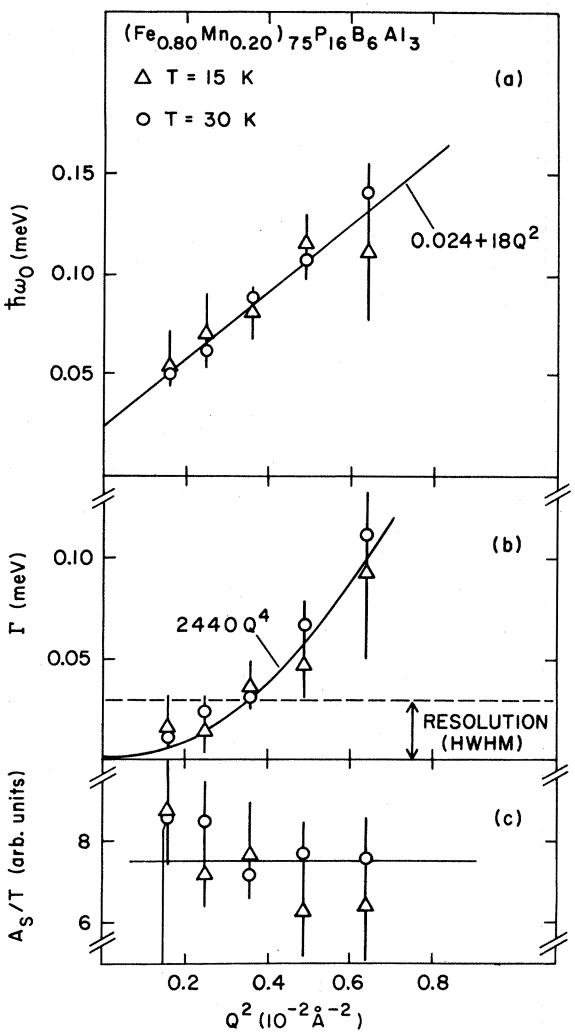

FIG. 14. Q dependence of parameters describing inelastic component of spectra near and below the FM-SG crossover for $x=0.20$.

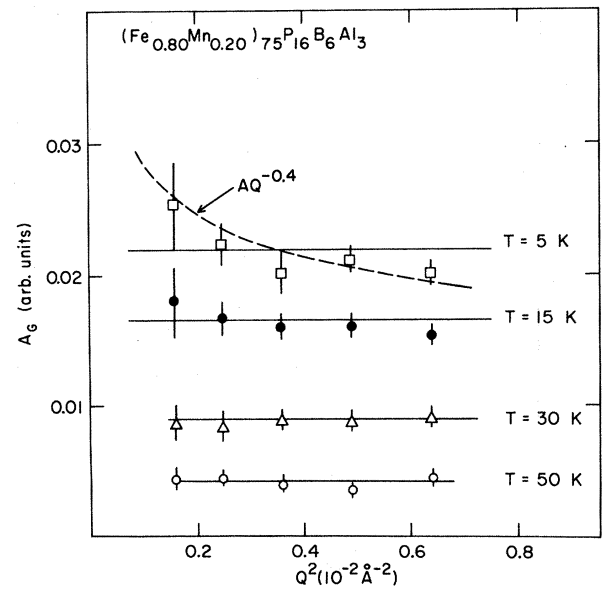

FIG. 15. Q dependence of quasielastic peak amplitude A_G. Horizontal lines correspond to quasielastic intensities decaying according to a Q^{-2} law.

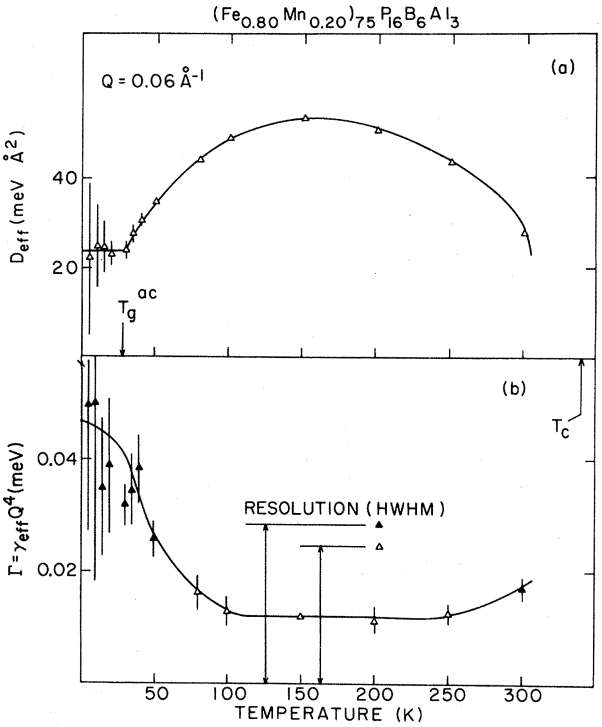

FIG. 16. Temperature dependence of parameters D_{eff} and $\Gamma=\gamma_{\text{eff}}Q^4$ describing $Q=0.06$ Å^{-1} spectra for $x=0.20$. T_g^{ac} is the temperature given by bulk measurements[3] for the FM-SG crossover. T_C is from our neutron scattering data (see Table I).

In addition to the medium-resolution survey discussed above, we have carried out some high-resolution ($\Delta E=26$ μeV FWHM) measurements at temperatures below 30 K. The important result is that in all of the spectra collected, the central peak is resolution limited. We conclude that in the RSG regime, this peak must be caused by spin fluctuations with relaxation times exceeding 10^{-9} sec.

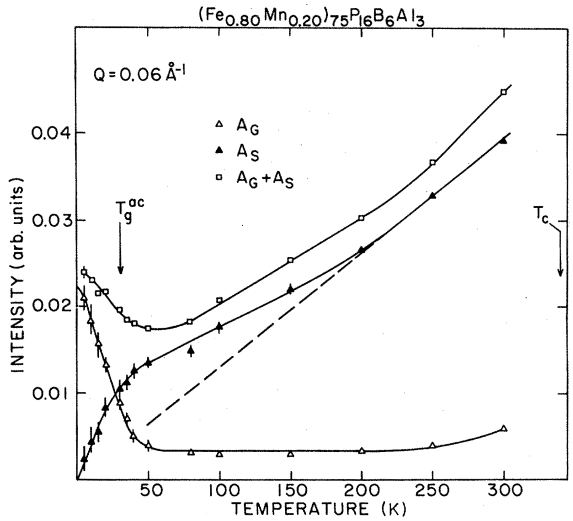

FIG. 17. Temperature dependence of integrated spin-wave intensity (A_S), quasielastic peak amplitude (A_G), and net scattering amplitude (A_G+A_S), for $Q=0.06$ Å^{-1} and $x=0.20$.

V. DISCUSSION

A. Dynamics of spin-glasses and random ferrimagnets

Considerable theoretical literature exists on the dynamics of spin glasses without higher-temperature ferromagnetic phases.[24–27] The conventional analytical wisdom is that at long wavelengths, propagating spin waves with a linear dispersion law should exist, as in other systems, such as antiferromagnets, where the order parameter does not commute with the Hamiltonian. However, computer simulations of Heisenberg spin-glasses described by the Hamiltonian (7) where J_{nm} is a random variable with zero mean, have produced no evidence for such modes.[27]

Much less work exists on the dynamics of ferromagnets which display spin-glass-like behavior at low temperatures. Halperin and Saslow briefly considered the hydrodynamic modes in what may be called a random ferrimagnet.[24] Such a system is characterized by both a nonvanishing net magnetization and random static fluctuations in the spin direction and displays two kinds of (gapless) hydrodynamic modes. Not surprisingly, the first is an SG-like mode with linear dispersion law, while the second corresponds to ferromagnetic magnons with quadratic dispersion. Fischer[28] has recently studied the dynamics of the random ferrimagnet in greater detail and reached essentially the same conclusions as Halperin and Saslow. However, he also found that the ferromagnetic mode, even while retaining its quadratic dispersion, can be damped *quadratically* rather than quartically, as is usually the case. We add parenthetically that Gabay and Toulouse[29] have found that the reentrant SG state discovered by Sherrington and Kirkpatrick[30] (SK) for their Ising model becomes a random ferrimagnet in the Heisenberg version of the SK model.

On the numerical side, Krey[31] has performed a study of the $T=0$ spectral function $S(\vec{Q},\omega)$ for $Eu_xSr_{1-x}S$. In this work, very broad peaks, with positions described by a *ferromagnetic* dispersion law, were found at large momenta $\vec{Q}$. As $|\vec{Q}|$ was decreased below 0.4 (in reduced lattice units), the widths of these peaks became comparable to their energies, and the primary feature in $S(\vec{Q},\omega)$ was an intense quasielastic peak, as seen in the inelastic neutron scattering measurements.[7] Again there was no evidence for a propagating spin-wave mode obeying a linear dispersion law at small $\vec{Q}$.

The inelastic spectra for $(Fe_{1-x}Mn_x)_{75}P_{16}B_6Al_3$ in the RSG regime are very similar to those computed for $Eu_xSr_{1-x}S$ by Krey. Namely, we find sharp quasielastic peaks coexisting with inelastic scattering which can be attributed to highly damped ferromagnetic spin waves. Of course, our data are also consistent with the analytical results for a random ferrimagnet, where a highly damped FM-like spin-wave mode is predicted. However, the bulk measurements indicate the absence of a net FM moment at the lowest temperatures. Hence it is unlikely that the inelastic scattering in the RSG regime is due to true FM modes. At higher temperatures, spin-wave peaks coexist with resolution-limited quasielastic scattering (see Fig. 10), and the FM moment is nonvanishing. Here it would be more reasonable to identify the magnetic state as a random ferrimagnet, or equivalently, a Gabay-Toulouse (GT) state. Within this interpretation,[6] the central peak in our spectra corresponds to randomly frozen spin fluctuations, while the inelastic peaks are derived from the hydrodynamic spin waves associated with the net FM moment. Needless to say, the phase diagram shown in Fig. 1 would be complicated by the addition of a boundary separating RSG from Gabay-Toulouse states. Also, random-field effects, as described in paper I, would destroy the FM order in the GT state, and thus make the GT and RSG states indistinguishable.

An important conclusion of the analytical work is that in spin-glasses and random ferrimagnets, there is a (Heisenberg) symmetry restoring mode obeying the linear dispersion law $\hbar\omega_0=c\,|\vec{Q}|$. We have found no evidence for such a mode (with $c\neq 0$) in the ferromagnetic and spin-glass regimes of all four of our samples. There is of course always the possibility that such a mode actually exists at very small $\vec{Q}$, but that it is overdamped in the range of momentum transfers accessible in our experiments. Another interpretation is that our experimental resolution is too coarse, and the order-parameter scattering at $\omega=0$ too strong, to allow direct observation of the Halperin-Saslow modes. However, if the modes were to exist, an applied magnetic field H would lift the degeneracy between them to yield two excitation branches. The results are the same as for an antiferromagnet in an applied field. For small H, the first mode is still described by $\hbar\omega_0=c\,|Q|$, while the second is characterized by the dispersion relation

$$\hbar\omega_0=[(g\mu_B H)^2+(cQ)^2]^{1/2}\,. \tag{32}$$

If this second branch is indeed what we have observed for $x=0.35$ at finite fields (Fig. 3), we can place an upper bound of 2 meV Å on c.

B. Random-field model and spin dynamics

In paper I, we presented a model for the crossover from ferromagnetic to spin-glass behavior in random magnetic alloys like $(Fe_{1-x}Mn_x)_{75}P_{16}B_6Al_3$. The model is based on a decomposition of the spin system into spin-glass (SG) and ferromagnetic (FM) networks, containing spins which we labeled as $\vec{\sigma}_i$ and $\vec{S}_j$, respectively. The SG network is defined to be frustrated with respect to the FM network. Operationally, this means that if the FM network is fully ordered, the ground state of the SG network is sufficiently degenerate so that a freezing process involving substantial relaxation times can occur among the $\vec{\sigma}_j$. Once this freezing occurs, the $\vec{\sigma}_i$ impose a random field on the $\vec{S}_j$. Random fields are known to destroy magnetic order in three-dimensional, short-range coupled systems. The magnetic Bragg reflections observed by neutron diffraction are converted into diffuse scattering of the form[17]

$$S(Q)=A\left[\frac{1}{Q^2+\kappa^2}\right]^2+B\left[\frac{1}{Q^2+\kappa^2}\right]\,. \tag{33}$$

Our random-field model for the SG-RSG crossover provides a natural explanation for many experimental features common to a wide variety of magnetic alloys, ranging from insulating $Eu_xSr_{1-x}S$ to metallic Fe_xCr_{1-x}.[1-8] In particular, it accounts for the nearly identical results obtained for all RSG alloys in quasielastic neutron scattering measurements. At first glance, the situation as far as neutron scattering studies of spin dynamics are concerned seems less universal. Thus far, only the inelastic measurements on the metallic systems Fe_xAu_{1-x},[5] Fe_xCr_{1-x},[4] $(Fe_{1-x}Ni_x)_{75}P_{16}B_6Al_3$,[6] and $(Fe_{1-x}Mn_x)_{75}P_{16}B_6Al_3$ have explicitly demonstrated the appearance, and subsequent disappearance of FM spin-wave peaks with decreasing T. However, these Fe-based alloys are also the RSG systems with by far the highest Curie temperatures. Furthermore, their low-temperature spectra, which consist of a sharp quasielastic peak coexisting with relatively broad inelastic scattering, are very similar to the inelastic spectra for $Eu_xSr_{1-x}S$.[7] We therefore believe that with improvements in spectrometer resolution and discoveries of insulating, or at least nonitinerant,[32] magnetic alloys with higher Curie temperatures, it will become apparent that the spin dynamics of RSG systems are as universal as the statics.

We turn now to the implications of our random-field model for the spin dynamics of RSG alloys. Recall that one can define the time-dependent generalization of the Edwards-Anderson order parameter for spins $\vec{\sigma}_i$ in the SG networks as

$$Q_{\mathrm{EA}}(t)=\langle \vec{\sigma}_i(0)\cdot\vec{\sigma}_i(t)\rangle \ . \tag{34}$$

For T above T_f, the glass transition temperature, $Q_{\mathrm{EA}}(t)$ at large t is characterized by some finite relaxation time τ_0, i.e.,

$$Q_{\mathrm{EA}}(t)=q_0\exp(-|t|/\tau_0) \ . \tag{35}$$

As discussed in paper I, Q_{EA} induces a random field on the spins $\vec{S}_i$ through the exchange bonds also responsible for frustration. For $T>T_g$, this random field h_i is *time dependent* and has autocorrelations

$$\langle \vec{h}_i(t')\cdot\vec{h}_j(t)\rangle = h^2\delta_{ij}\exp(-|t'-t|/\tau_0) \tag{36}$$

While there exists a substantial body of literature dealing with static random fields,[17] to our knowledge, no work exists on the subject of random fields with finite relaxation times. Consequently, we give here some speculations on the spin dynamics of a normal Heisenberg ferromagnet in the presence of time-varying random fields $\vec{h}(\vec{r},t)$ satisfying Eq. (36).

At wave vectors $\vec{Q}$ such that the inverse relaxation time τ_0^{-1} is considerably smaller than the spin-wave frequency $\omega_0(\vec{Q})$, the spins should respond to $\vec{h}(\vec{r},t)$ much as they would to a static random field. We therefore expect to see quasielastic scattering with $\vec{Q}$ dependence as given by formula (33). The width of an energy scan through this scattering should simply by the inverse autocorrelation time τ_0^{-1} for the random field. As far as the spin waves are concerned, they are propagating through a medium of randomly distributed static scattering centers. In analogy to many other situations where waves propagate through random media, we expect the lifetime of the spin waves here to decrease as the random-field amplitude rises.

For $\tau_0^{-1}\gg\omega_0(\vec{Q})$, the ferromagnetic network will respond as to any white (frequency-independent) noise. Specifically, as energy is transferred from the noise source to the ferromagnetic spins, the observed spin-wave amplitude will increase, and the magnetization and stiffness will decrease correspondingly.

We now apply these ideas about time-dependent random fields to the spin dynamics of RSG alloys like $(Fe_{1-x}Mn_x)_{75}P_{16}B_6Al_3$. As the temperature is reduced below T_C, the system should initially behave—at least in a qualitative sense—like an ordinary ferromagnet. This means that the magnetization M and spin-wave stiffness D will both increase, while the spin-wave amplitude A_s will decrease. Following the description of paper I, the SG spins $\vec{\sigma}_i$, when considered independently of the FM network, undergo a freezing process with some characteristic temperature $T_g<T_C$. Therefore, reductions in T should also lead to increases in the SG relaxation time τ_0. Let us consider the case where $T_g<T<T_C$ and τ_0^{-1} is larger than the energies of observable spin waves. The primary effect of increases in τ_0 will then be an increase in A_S relative to what it would be in the absence of coupling between SG and FM networks. There should be a corresponding decrease in M and D. Because of the competition between this effect and the ordering tendency of the FM network with decreasing T, we can expect a maximum in M and D at a temperature T_M between T_g and T_c.

No major qualitative change in the form of the inelastic spectra themselves needs to occur near T_M, as long as τ_0^{-1} is still larger than $\omega_0(\vec{Q})$. However, as T approaches the SG freezing point T_g, τ_0 must by definition become very large. Thus, for the relatively large $\vec{Q}$ studied in experiments such as ours, $\omega_0(\vec{Q})\gg\tau_0^{-1}$. According to our discussion of time-dependent random-field effects, the inelastic spectra in this case will display a quasielastic component, in addition to the usual spin-wave peaks. The quasielastic component should decay with $\vec{Q}$ according to the random-field form, Eq. (33), which at large $\vec{Q}$ is simply BQ^{-2}. Another important change which occurs as $T\to T_g$ is that the time-dependent random field, imposed by the SG network, appears static to the spin waves, with the result that the effective damping $\Gamma(\vec{Q})$ increases.

An important driving mechanism for the changes in the spin dynamics as T approaches T_g from above is the coupling between the relaxation processes among the SG spins and the spin waves in the FM network. Once SG order is established, i.e., the relaxation time τ_0 has diverged, the remnants of FM spin waves will of course still be coupled to the finite frequency excitations of the SG network. However, these excitations in pure, nonferromagnetic, spin-glasses are well known to have very low characteristic frequencies. Therefore, the spin-wave–like excitations among FM spins at $Q\gg\kappa$ will essentially be decoupled from the SG excitations. This implies that as T is reduced in the RSG phase, no substantial change in the parameters D and Γ describing the inelastic part of the spectra (for $Q\gg\kappa$) is expected. At the same time, the

amplitude A_S should simply be proportional to T. We emphasize that the observation of spin-wave-like features in neutron scattering spectra collected at finite Q by no means indicates the presence of long-range FM order, as has recently been suggested in the context of RSG behavior in Fe_xAu_{1-x}.[5]

The qualitative picture presented above is an excellent agreement with our data for the $x=0.25$ and 0.20 alloys. Notably, it accounts for the maximum in D which occurs at a temperature T_M well above the characteristic temperature T_g for the FM-RSG crossover. Furthermore, it explains why significant quasielastic scattering, obeying a Q^{-2} law is present at T larger than T_f but less than T_M. Finally, it provides some insight into why the spin dynamics do not change noticeably with $T < T_g$.

Very recently, Continentino[33] has considered a ferromagnet where the spin waves are coupled to an ensemble of two-level systems, which might represent the "decoupled clusters" in our treatment of the RSG problem. He also finds that the spin-wave energies and lifetimes decrease with T. However, because his model, unlike ours, does not explicitly couple *all three* "ferromagnetic" spin components to the two-level systems, he fails to predict the central peak which coexists with the spin-wave sidebands in our data.

Before concluding, we comment briefly on our field-dependent measurements for $x=0.35$. As the applied field H was increased from zero, most of the quasielastic scattering disappeared while inelastic sidebands developed at $E=\pm g\mu_B H$, independent of the momentum transfer. It is likely that this absence of noticeable dispersion arises because at this x, many spins reside in small ferromagnetically coupled clusters, frustrated with respect to each other. By small we mean smaller than the size corresponding to the largest momentum transfer ($Q=0.1$ Å^{-1}) probed.

VI. SUMMARY AND CONCLUSIONS

We have performed inelastic neutron scattering measurements on amorphous $(Fe_{1-x}Mn_x)_{75}P_{16}B_6Al_3$ for four manganese concentrations near the crossover from ferromagnetic to spin-glass-like behavior. Table I lists these concentrations, and corresponding spin-wave parameters and characteristic temperatures given by our data. For $x=0.35$, which is on the spin-glass side of the phase diagram (see Fig. 1), the spectra were dominated by a resolution-limited quasielastic peak, and no evidence was found for propagating modes. The other samples ($x=0.30$, 0.25, and 0.20) were on the ferromagnetic side of the phase diagram. For all three, resolvable spin-wave peaks were observed at intermediate temperatures. Furthermore, simple spin-wave theory gave an excellent account of the $\vec{Q}$ dependence of the inelastic spectra. However, the temperature dependence of the spin-wave parameters was not in accord with simple theory. For example, the spin-wave stiffness was found first to increase, and then to decrease as T was reduced. As the spin-glass regime was approached, resolvable spin-wave peaks disappeared altogether, and the spectra resembled those for the nonferromagnetic spin glass with $x=0.35$. Accordingly, the principal component of the low-temperature scattering was a resolution-limited quasielastic peak. For the most iron-rich sample ($x=0.20$), true inelastic scattering supplemented this central peak, even at 5 K. Furthermore, direct inspection of the data near the FM-SG crossover showed the coexistence of quasielastic magnetic scattering with well-resolved spin-wave peaks. Over the range of momentum transfers probed ($0.04 \leq Q \leq 0.08$ Å^{-1}), the central peak intensity I always decayed according to a power law $Q^{-\alpha}$ with $\alpha \geq 2$.

Our previous paper, which dealt with the instantaneous spin correlations in $(Fe_{1-x}Mn_x)_{75}P_{16}B_6Al_3$, contained a heuristic model, based on random-field effects, for the FM-SG crossover. In the present paper, we have discussed the implications of this model for the spin dynamics of RSG alloys. The reduction of the spin-wave stiffness with temperature, and the appearance of a central peak in the spectra are easily explained within the context of our random-field model. We emphasize that in the ferromagnetic regime, the random field in question is *time dependent,* and the FM-SG crossover occurs because the autocorrelation time for this random field becomes very large.

Considerable work on RSG dynamics remains to be done. On the experimental side, ultrahigh resolution neutron scattering measurements of the central peak in an alloy such as $(Fe_{0.80}Mn_{0.20})_{75}P_{16}B_6Al_3$ would be very interesting. According to our random-field model, this peak should acquire a finite width in energy which grows with temperature above the SG-FM crossover. On the theoretical side, studies of spin dynamics in both static and time-varying fields are clearly needed.

ACKNOWLEDGMENTS

We thank R. Bruinsma for helpful conversations, and R. Youngblood for providing the Monte Carlo integration routine used in our data analysis. We are also grateful to J. Lynn for sending us a copy of an unpublished paper reporting his group's recent work on $(Fe_xNi_{1-x})_{75}P_{16}B_6Al_3$. Work at Brookhaven National Laboratory was supported by the Division of Materials Sciences, U.S. Department of Energy, under Contract No. DE-AC02-76CH00016. Work at Massachusetts Institute of Technology was supported by the National Science Foundation under Grant No. DMR-79-23203.

[1]G. Aeppli, S. M. Shapiro, R. J. Birgeneau, and H. S. Chen, Phys. Rev. B 28, 5160 (1983). See also G. Aeppli, Ph.D. thesis, Massachusetts Institute of Technology, 1982 (unpublished).

[2]Y. Yeshurun, M. B. Salamon, N. V. Rao, and H. S. Chen, Phys. Rev. Lett. 45, 1366 (1980).

[3]J. A. Geohegan, S. M. Bhagat, J. Magn. Magn. Mater. 25, 17 (1981).

[4]S. M. Shapiro, C. R. Fincher, A. C. Palumbo, and R. D. Parks, Phys. Rev. B 24, 6661 (1981).

[5]A. P. Murani, Phys. Rev. B 28, 432 (1983).

[6]J. W. Lynn, R. W. Erwin, H. S. Chen, and J. J. Rhyne, Solid State Commun. 46, 317 (1983).

[7]H. Maletta, W. Zinn, H. Scheuer, and S. M. Shapiro, J. Appl.

Phys. 52, 1735 (1981).
[8]H. Maletta, G. Aeppli, and S. M. Shapiro, Phys. Rev. Lett. 48, 1490 (1982).
[9]W. Marshall and S. W. Lovesy, *Theory of Thermal Neutron Scattering* (Oxford University Press, London, 1971).
[10]K. Kawasaki, Prog. Theor. Phys. 38, 1052 (1967).
[11]B. I. Halperin and P. C. Hohenberg, Phys. Rev. 177, 952 (1969).
[12]L. Passell, J. Als-Nielsen, and O. W. Dietrich, in *Proceedings of the Fifth IAEA Symposium on Neutron Inelastic Scattering* (IAEA, Vienna 1972), p. 619.
[13]A. B. Harris, Phys. Rev. 175, 674 (1968), and references therein.
[14]See, for example, D. Forster, *Hydrodynamic Fluctuations, Broken Symmetry, and Correlation Functions* (Benjamin, Reading, 1975).
[15]O. W. Dietrich, J. Als-Nielsen, and L. Passell, Phys. Rev. B 14, 4923 (1976); M. F. Collins, R. Nathans, L. Passell, and G. Shirane, Phys. Rev. 179, 417 (1969); J. A. Tarvin, G. Shirane, R. J. Birgeneau, and H. S. Chen, Phys. Rev. B 17, 241 (1978); J. D. Axe, G. Shirane, T. Mizoguchi, and H. Yamauchi, *ibid.* 15, 2763 (1977).
[16]A. Tucciarone, H. Y. Lau, L. M. Corliss, A. Delapalme, and J. M. Hastings, Phys. Rev. B 4, 3206 (1971).
[17]G. Parisi and N. Sourlas, Phys. Rev. Lett. 43, 744 (1979), and references therein; Y. Imry and S.-k. Ma, *ibid.* 35, 1399 (1975); H. S. Kogon and D. J. Wallace, J. Phys. A 14, L527 (1981); H. Yoshizawa, R. A. Cowley, G. Shirane, R. J. Birgeneau, H. J. Guggenheim, and H. Ikeda, Phys. Rev. Lett. 48, 438 (1982).
[18]S. F. Edwards and P. W. Anderson, J. Phys. F 5, 965 (1975).
[19]A. P. Murani and A. Heidemann, Phys. Rev. Lett. 41, 1402 (1978).
[20]See W. Kinzel (unpublished) for a review.
[21]A. P. Murani, J. Magn. Magn. Mater. 22, 271 (1981).
[22]H. Sompolinsky, Phys. Rev. Lett. 47, 935 (1981).
[23]N. J. Chesser and J. D. Axe, Acta Crystallogr. Sect. A 29, 160 (1973).
[24]B. I. Halperin and W. M. Saslow, Phys. Rev. B 16, 2154 (1977).
[25]S. F. Edwards and P. W. Anderson, J. Phys. F 6, 1927 (1976).
[26]D. L. Huber and W. Y. Ching, in *Amorphous Magnetism II*, edited by R. A. Levy and R. Hasegawa (Plenum, New York, 1977), p. 39.
[27]W. Y. Ching, K. M. Leung, and D. L. Huber, Phys. Rev. Lett. 39, 729 (1977).
[28]K. H. Fischer, Z. Phys. B 38, 243 (1980).
[29]M. Gabay and G. Toulouse, Phys. Rev. Lett. 47, 201 (1981).
[30]D. Sherrington and S. Kirkpatrick, Phys. Rev. Lett. 35, 1792 (1975).
[31]U. Krey, Z. Phys. B 38, 243 (1980).
[32]F. J. Litterst, J. M. Friedt, J. L. Tholence, and F. Holtzberg, J. Phys. C 15, 1049 (1982).
[33]M. Continentino, Phys. Rev. B 27, 4351 (1983).